Constraints on ocean circulation at the Paleocene-Eocene Thermal Maximum from neodymium isotopes

April N. Abbott[1], Brian A. Haley[1, 2] Aradhna K. Tripati[3,4], Martin Frank[2]

1. CEOAS, OSU, 104 Ocean Admin. Bldg., Corvallis, OR 97209, USA
2. GEOMAR Helmholtz Centre for Ocean Research Kiel, Wischhofstrasse 1-3, 24148 Kiel, Germany
3. Department of Earth and Space Sciences, Department of Atmospheric and Oceanic Sciences, and Institute of the Environment and Sustainability, University of California, Los Angeles, CA 90095, USA
4. European Institute of Marine Sciences (IUEM), Université de Brest, UMR 6538, Domaines Océaniques, Rue Dumont D'Urville, Plouzané, France

Corresponding author: bhaley@coas.oregonstate.edu

ABSTRACT

Global warming during the Paleocene Eocene Thermal Maximum (PETM) ~55 million years ago (Ma) coincided with a massive release of carbon to the ocean-atmosphere system, as indicated by carbon isotopic data. Previous studies have argued for a role for changing ocean circulation, possibly as a trigger or response to climatic changes. We use neodymium (Nd) isotopic data to reconstruct short high-resolution records of deep-water circulation across the PETM. These records are derived by reductively leaching sediments from seven globally distributed sites and comparing data with published data from fossil fish debris to reconstruct past deep ocean circulation across the PETM. The Nd data for the leachates are interpreted to be consistent with previous studies that have used fish teeth and benthic foraminiferal $\delta^{13}C$ to constrain regions of convection. There is some evidence from combining Nd isotope and $\delta^{13}C$ records that the three major ocean basins may not have had substantial exchanges of deep waters. If the isotopic data are interpreted within this framework, then the observed pattern may be explained if the strength of overturning in each basin varied distinctly over the PETM, resulting in differences in deep-water aging gradients between basins. Results are consistent with published interpretations from proxy data and model simulations that suggest modulation of overturning circulation had an important role for global recovery of the ocean-atmosphere system after the PETM.

1.0 Introduction

The PETM represents a time of profound global change with deep sea temperatures increasing 4-8°C (Katz et al., 1999; Kennett and Stott, 1991; Sluijs et al., 2006; Tripati and Elderfield, 2004, 2005; Zachos et al., 2001, 2003, 2006), widespread biological extinctions (e.g. Kennett and Stott, 1991), and ocean acidification marked by widespread carbonate dissolution occurring ~ 55 Ma (Dickens, 2000; Kump et al. 2009; Ridgwell and Schmidt, 2010; Zachos et al., 2005, 2008; Zeebe and Zachos, 2007). In general, the timing and global distribution of temperature records across the PETM are consistent with strong greenhouse forcing (Kennett and Stott, 1991; Tripati and Elderfield, 2004, 2005; Zachos et al., 2001, 2003; Sluijs et al., 2007) although the amount of carbon released, the type of carbon (Zeebe et al., 2009), and the possible role of other forcing agents (e.g., water vapor, aerosol loading, surface albedo feedbacks) is unclear (Bowen et al., 2004; Lunt et al., 2012). Changes in deep ocean circulation, orbital cycles, and volcanic exhalations are proposed causes of the initial warming (e.g., Kennett and Stott, 1991; Bice and Marotzke, 2002; Dickens et al., 1995; Lunt et al., 2011, 2012; McInerney and Wing, 2011 Nunes and Norris, 2006; Sluijs et al., 2007; Tripati and Elderfield, 2005; Winguth et al., 2010; Zachos et al., 2001). Climate simulations even suggest that the magnitude and pacing of the PETM and subsequent smaller events (ETM2 and ETM3) can be explained by orbitally induced changes in water temperature and circulation controlling the destabilization of methane hydrates (e.g. Lunt et al., 2010).

A striking characteristic of the PETM is a pronounced global negative stable carbon isotope ($\delta^{13}C$) excursion (CIE) (Kennett and Stott, 1991; Koch et al., 1992; Bowen et al., 2001; Nunes and Norris, 2006; McCarren et al., 2008; McInerney and Wing, 2011; Zachos et al., 2001). This isotopic excursion resulted from a rapid release (in less than 10,000 years) of carbon

68 from an isotopically light reservoir, likely resulting from the warming climate (e.g., Farley and
69 Eltgroth, 2003; Murphy et al., 2010; Röhl et al., 2007). Based on basinal gradients of available
70 benthic $\delta^{13}C$ data (Nunes and Norris, 2006; Tripati and Elderfield, 2005), widespread carbonate
71 dissolution (Dickens, 2000; Kump et al. 2009; Ridgwell and Schmidt, 2010; Zachos et al., 2005,
72 2008), inferred deep-sea carbonate ion gradients (Zeebe and Zachos, 2007), as well as numerical
73 modeling studies (Bice and Marotzke, 2002; Lunt et al., 2012), it has been argued that a change
74 in thermohaline circulation may have been associated with the PETM. Such studies have
75 postulated circulation regimes fundamentally different than the modern ocean operating before
76 and after the PETM (Kennett and Stott, 1991, Lunt et al., 2011). Specifically, studies have
77 proposed the existence of Southern Ocean deep-water formation (Kennett and Stott, 1991) based
78 on high-resolution carbon isotope records that are used to infer basinal deep-water aging
79 gradients (Nunes and Norris, 2006; Tripati and Elderfield, 2005) and have suggested intermittent
80 deep water formation in the North Pacific based on a fully coupled atmosphere-ocean general
81 circulation model based on pCO2 simulations (Lunt et al., 2011). It is hypothesized that due to
82 gradual changes in the temperature and hydrology of high-latitude surface waters, these
83 southern-sourced waters were displaced during the PETM with the development of convection in
84 the northern hemisphere (Alexander et al., 2015; Bice and Marotzke, 2002; Nunes and Norris,
85 2006; Tripati and Elderfield, 2005). The combination of warmer deep water and circulation
86 changes may have served as a trigger or amplifier of the massive carbon release that resulted in
87 the global CIE, possibly through the destabilization of methane hydrates (e.g. Bice and
88 Marotzke, 2002; Lunt et al., 2011).
89 However, interpreting past benthic $\delta^{13}C$ records in benthic foraminifera of the PETM as a
90 strict indicator of thermohaline circulation is complicated by possible contributions of

fractionated carbon sources (Kurtz et al., 2003), changes in marine productivity (Paytan et al., 2007), deep water carbon export (McCarren et al., 2008), extinction and migration events of the biota, and potential signal loss through dissolution in highly corrosive bottom waters (Alexander et al., 2015; McCarren et al., 2008; Pagani et al., 2006; Zeebe and Zachos, 2007). In contrast, the geochemical cycling of Nd in the oceans allows Nd isotopes to be used as a quasi-conservative tracer of water mass distributions that is generally not affected by biogeochemical processes that can be used to reconstruct past ocean circulation (e.g., Frank, 2002; Goldstein et al., 2003; Thomas, 2004).

Published records of past seawater Nd isotope compositions (ε_{Nd}) extracted from fossil fish teeth serve as a quasi-conservative proxy for past deep-water mass distributions and mixing and do not show evidence for changes at the PETM. Specifically, the low-resolution ε_{Nd} data from fish teeth have been interpreted as possibly reflecting an uninterrupted contribution from a Southern Ocean deep-water source in multiple basins across the PETM (Thomas et al., 2003). This apparent disparity between proxy data may reflect the non-conservative nature of interpreting benthic foraminiferal $\delta^{13}C$, or could arise from the low-resolution nature of the published Nd isotope records.

To address whether there is Nd isotope evidence for changes in water mass distributions, we developed high-resolution records of the ε_{Nd} composition of Fe-Mn leachates from seven sites and compare these results to published ε_{Nd} data for fish teeth (Thomas et al., 2003) and benthic foraminiferal $\delta^{13}C$ (Nunes and Norris, 2006; Tripati and Elderfield, 2005; Zachos et al., 2001). The Nd isotope composition of Fe-Mn oxide leachates from core-top sediments has been used to accurately reconstruct bottom water values (Rutberg et al., 2000; Bayon et al., 2002; Gutjahr et al., 2007). This technique has also been applied to downcore sediments to study

114 variations in bottom water circulation during the Pleistocene (Rutberg et al., 2000; Piotrowski et
115 al., 2004, 2005, 2008). Measurements on older sediments ranging from Cenozoic (Martin et al.,
116 2010) to Cretaceous (Martin et al., 2012) in age has shown that sequences from multiple
117 localities can preserve a Nd isotope signal similar to fish teeth and can be used to develop much
118 higher-resolution paleoceanographic records.
119
120 **2. Materials and Methods**
121 *2.1 Sample and locality information*
122 Details on the core locations, depths and paleo-depths are given in Table 1. Sites were
123 located at similar water depths during the PETM, with paleodepths between 2400 and 3200 m in
124 the Pacific, between 1900 and 2000 m in the North Atlantic, and between 1900 and 3400 m in
125 the Southern and Indian Oceans (Table 1). Sources for the carbon isotope data referred to in this
126 study is reported in this table. The age models used to plot all the data (including $\delta^{13}C$) are
127 shown in Table 2, and are derived from the information given in the publications of the $\delta^{13}C$ data
128 (Thomas et al., 2003; Nunes and Norris, 2006; Tripati and Elderfield, 2005). For completeness,
129 we show in Table 2 the core depth-age curve fits that describe the age models for each core,
130 where:
131 $$\text{Age (Myr)} = m(\text{Core Depth in mbsf}) + b.$$
132 Several segments are listed if sedimentation rates varied down core (the depth ranges of
133 these segments are listed in Table 2). In all cases, simple linear sedimentation rates were used.
134 These age models were also used to calculate the ages used here for the fish teeth/debris data
135 (Thomas et al., 2003).
136

2.2 Sample preparation

Freeze-dried sediment samples were obtained from the Integrated Ocean Drilling Program (IODP). One to two grams dry weight of sediment was then rinsed with ultra-high purity (Milli-Q) water, and then processed following established sediment leaching protocols (e.g., Bayon et al., 2002, 2004; Haley et al., 2008a; Jacobsen and Wasserburg, 1979; Martin et al., 2010; Piotrowski et al., 2008; Rutberg et al., 2000; Scher and Martin, 2006). Briefly, we thoroughly rinse the sediments with Milli-Q water, leach with buffered acetic acid for 2.5 hours and collect the leachate, then rinse thoroughly with Milli-Q again before the reduction of early diagenetic metal oxide coatings that carry the bottom water Nd isotope signatures with a dilute buffered hydroxylamine.HCl-acetic acid solution. This buffered hydroxylamine.HCl-acetic acid solution leaches the authigenic metal oxide coatings, which are then removed from the sediment and run through standard chromatographic procedures to extract a pure Nd solution for mass spectrometric analyses (AG 50W X12 resin for cation separation followed by di-2-ethylexyl-phosphate resin for rare earth element separation; see Gutjahr et al. 2007 for details). Many of the initial acetic leachates were run through the same chromatographic procedures for the same Nd analysis. ε_{Nd} of the first (buffered acetic) and second (hydroxylamine.HCl) leachates were dominantly within error of each other (0.5 ε_{Nd}), thus we consider our hydroxylamine.HCl leaches to reliably reflect bottom water signatures. The reliability of these signatures is further supported by recent publications demonstrating the validity of hydroxylamine.HCl leaches in the absence of volcanic material (e.g. Khélifi and Frank, 2014; Böhm et al., 2015). Still potential uncertainties are associated with leaching sediments that may have undergone late stage diagenesis, although to our knowledge no concrete examples exist in the literature for the influence of late stage diagenesis on the recorded εNd signature. For this reason we focus our

interpretations on the relative changes in the Nd isotope signature rather than on absolute values. All sediments that could be sampled from the seven sites were analyzed and are presented here. No additional sediment was available to alter or repeat the leaching procedure after our original analysis (pre 2012) to account for new findings in leaching methods (Molina-Kescher et al., 2014; Wilson et al., 2012).

2.3 Sample analysis

Nd was analyzed on two instruments: a Triton Thermal-Ionization Mass Spectrometer at IFM-GEOMAR, using $^{146}Nd/^{144}Nd = 0.7219$ to correct for instrument fractionation, and a Nu Instruments multi-collector inductively coupled mass spectrometer at Oregon State University. Nd isotopes are expressed in ε_{Nd} notation, defined as the deviation of measured $^{143}Nd/^{144}Nd$ ratios from a bulk Earth value of CHUR (chondritic uniform reservoir) in the 5th decimal place (Thomas et al., 2003). Long-term reproducibility of a Nd standard solution (SPEX source) gave a 2σ error of 0.5 ε_{Nd} units representing the total error of analyses and normalization, exactly as the samples. Analyses of the JNdi standard used for normalization had a lower 2σ error of 0.3 ε_{Nd} units. Nd isotope data are not corrected for decay of samarium given the limited temporal range of the data and the lack of constraints on sample Sm/Nd isotope ratios. Nd isotope corrections for the PETM are typically small (<0.5 ε_{Nd} units; Thomas et al. 2003) and therefore do not influence our interpretations.

3. Results and Discussion

We have applied a leaching technique (Gutjahr et al., 2007; Haley et al., 2008a; Haley et al., 2008b; Rutberg et al., 2000) that allows the extraction of past bottom water Nd isotope

183 compositions from the Fe-Mn oxide component of marine sediments, expressed as ε_{Nd} units
184 (Jacobsen and Wasserburg, 1979). Such data can provide high-resolution records of changes in
185 past deep-water mass mixing and used to interpret changes in circulation (Martin et al., 2010,
186 2012; Piotrowski et al., 2004, 2005, 2008; Thomas et al., 2014). Below we compare results from
187 leachates to data from fish teeth. We also compare results to carbon isotope data from the same
188 cores. By combining high-resolution ε_{Nd} and benthic $\delta^{13}C$ records from the same locations it is
189 possible to elucidate the causes and controls of $\delta^{13}C$ variations in the past deep oceans
190 (Piotrowski et al., 2005). Our new isotopic Nd data are combined with existing $\delta^{13}C$ records and
191 published Nd isotope data from fossil fish teeth of the Atlantic, Indian and Southern Oceans
192 (Thomas et al., 2003), in order to reconstruct global Nd isotope distributions across the PETM at
193 a resolution comparable to the corresponding $\delta^{13}C$ data (Figure 1).
194
195 *3.1 Comparison of neodymium isotope data obtained using different archives*
196 Consistent with published results for a number of different sedimentary environments
197 (Martin et al., 2012), we find evidence (Figure 1) for a general agreement between Nd isotopic
198 data from sediment leaches and fish teeth (Thomas et al., 2003). There appears to be a small,
199 possibly systematic offset at Site 401, and at 690B. This may be the result of higher-order
200 variability at these locations, or the result of a temporal difference between the uptake or the
201 retention of Nd in teeth and the ferromanganese coatings during sedimentation and diagenesis, or
202 a combination of the two. In the first instance, model studies (Lunt et al., 2011; Winguth et al.,
203 2010) have confirmed that locations near the Antarctic continent, such as at Site 690B, were
204 sensitive to changes in climate conditions, and, as such, likely to have varied more substantially
205 during the PETM (55.14-55.23 Ma for this study based on the CIE; Figure 2). Due to limited

206 constraints of the offsets between fish teeth and leach records, we focus our interpretations on the
207 relative trends in the ε_{Nd} signatures and their relation to the CIE.
208
209 *3.2 Broad patterns in Nd isotope records*
210 The broad patterns in these data support previous studies that have inferred convection
211 occurred in the Southern Ocean, and that convection occurred in both the North and South
212 Pacific during the PETM. The ε_{Nd} records cover the three major ocean basins (Figure 2) and
213 reveal distinct and basin-specific changes in deep circulation across the PETM. These data
214 suggest that a change in ocean circulation may have triggered the carbon release associated with
215 the PETM. Specifically, leachate ε_{Nd} records from Pacific Site 1220 show a negative excursion
216 of ~2 units prior to the CIE while fish teeth ε_{Nd} records indicate a similarly sized excursion in the
217 Southern Ocean.
218 Southern Sites 527 (subtropical South Atlantic) and 690 (Atlantic sector of the Southern
219 Ocean) fluctuated (1 to 1.3 ε_{Nd} units) around a mean ε_{Nd} of ~ -9 throughout the record, with
220 indications of a switch to in-phase co-variation during and after the PETM, also reflected by the
221 evolution of Site 213 (Figure 2). The ε_{Nd} records for eastern North Atlantic Site 401 stabilize at
222 ~ -9.3 during the PETM and then at ~ -8.2 post-PETM, with the trend towards radiogenic values
223 occurring at the end of the PETM. While the fish teeth ε_{Nd} record is not a step-function, the
224 observed magnitude and direction of change in leachate ε_{Nd} signatures is consistent with those
225 changes reported from fish teeth ε_{Nd} signatures (Thomas et al., 2003) (Figure 2). Deep waters at
226 central (western) Atlantic Site 1051B, located near the proto-Caribbean, had a more positive ε_{Nd}
227 (~-8) than Site 401 prior to the PETM, but post-PETM ε_{Nd} from both sites converged. The

228 record from Site 1051B exhibits similarities to post-PETM data from Site 401, which could
229 reflect more intense mixing within the North Atlantic following the recovery (Figure 2). Pacific
230 sites 1209B and 1220B were more radiogenic than the other basins (ε_{Nd} from -6 to -2). With the
231 exception of one data point (-2.1 ε_{Nd} at 55.02 Ma), the western Pacific (Site 1209B) had a
232 remarkably constant ε_{Nd} signature of -3.7 pre- and post-PETM. In contrast, the eastern Pacific
233 (Site 1220B) ε_{Nd} shows a short excursion from ~-4 to ~-5.5 ε_{Nd} at the onset of the PETM and
234 remained near unradiogenic end member values post-PETM (ε_{Nd} = -5) (Figure 2).
235
236 *3.3 A conceptual model to explain the records*
237 The dissimilarities between the ε_{Nd} records confirm that the globally similar CIE
238 dominantly reflects a change in source of oceanic carbon (Thomas et al., 2002). This change is
239 not directly from a volcanic or extra-terrestrial source, as these would also be seen the ε_{Nd} records
240 (Cramer and Kent, 2005). However, the ε_{Nd} data also clearly indicate that changes in water mass
241 distributions and mixing were associated with the PETM and suggest a fundamentally different
242 circulation system than present, with intermittent deep-water formation in the North Pacific,
243 must have existed during the PETM if we interpret the ε_{Nd} record as strictly indicative of
244 circulation. Without a change in circulation, we would expect that the εNd signals would remain
245 constant over the entire record or show a slow and predictable trend with any changes other than
246 circulation that may have occurred simultaneously (e.g. differing weathering inputs). Figure 3
247 illustrates our reconstruction of the evolution of global deep-water mass exchange during the
248 PETM, based on the interpretation of the global ocean as three distinct deep-water basins: the
249 "Southern Ocean," the North Atlantic and the Pacific. While in this model we hypothesize the

basins only had restricted water mass exchange between them, we cannot eliminate the possibility of unrestricted exchange since similar scale inter-basinal differences in ε_{Nd} are observed in the modern ocean without this restriction.

This conceptual model, based on both $\delta^{13}C$ and ε_{Nd} data, supports changes in areas of convection that are consistent with simulations of the PETM with coupled climate models (Lunt et al., 2012, Thomas et al., 2014) and with a comprehensive climate model (Winguth et al., 2010). It is impossible to interpret from the Nd isotope data alone whether there was reduced or increased overturning associated with carbon release, as these data reflect water mass geometries and not rates of overturning. It is of note that model simulations support a weakening of the meridional overturning circulation with increased greenhouse gases, which might result in a water mass geometry similar to what is reconstructed. However, changes in the exchange between ocean basins will be dependent on several factors, including buoyancy-induced and wind-stress induced changes in overturning, as well as topography. Below we discuss whether there is evidence for changes in ventilation from basinal deep-water aging gradients, and what the nature of topographic barriers may have been to produce the observed patterns in the data.

3.3.1. Southern records

An ε_{Nd} signature of -9.2 in the "Southern Ocean" most likely reflects an Antarctic margin source, similar to present day Antarctic-sourced intermediate waters (Stichel et al., 2012; Thomas et al., 2003). In agreement with previous inferences from $\delta^{13}C$ data (Tripati and Elderfield, 2005; Zeebe and Zachos, 2007), such a deep-water source can readily explain the post-PETM similarity of the ε_{Nd} records from both the Southern Atlantic (Site 527) and Indian Ocean (Site 213) with the Atlantic sector of the Southern Ocean (Site 690) (Figure 3). There are

indications that the co-variation of ε_{Nd} at Sites 213, 527, and 690 was enhanced immediately before, during, and following the PETM, which could be consistent with intensification of Southern Ocean-sourced ventilation (Figure 2a). Furthermore, ε_{Nd} signatures from fish teeth from site 690 and 527 suggest rapid changes in circulation leading into and during the early part of the PETM (Figure 1). The previously proposed formation of low-latitude Tethyan deep-water (e.g., Cope and Winguth, 2011; Huber and Sloan, 2001), or slower overturning circulation (Winguth et al., 2010) are unlikely to have generated such range and similarity in evolution of ε_{Nd} signatures at these three sites. Furthermore, numerical simulations indicate strong overturning circulation with multiple deep convection sites provide the best match to the ε_{Nd} record (Thomas et al., 2014).

3.3.2. Atlantic Ocean records

The contrast in ε_{Nd} trends between the Southern Ocean ε_{Nd} records and those of the North Atlantic (Figure 2) indicates that there was little exchange between these basins. The young Mid-Atlantic Ridge (MAR) between Africa and South America most likely represented an efficient barrier for north-south intermediate and deep-water exchange (Bice and Marotzke, 2002). This hypothesis differs from previous interpretations of overturning circulation in the Atlantic (Bice and Marotzke, 2002; Nunes and Norriz, 2006; Thomas et al., 2003), but confirms recent modeling results (Winguth et al., 2010). The differences between the two North Atlantic ε_{Nd} records can be readily explained by a weak North Atlantic deep-water overturning cell, resulting in higher sensitivity to local changes in Nd inputs or locally variable deep-water masses. Assuming weak, low-latitude, halothermally-driven downwelling in the North Atlantic

basin, we would expect Site 401 to show a different ε_{Nd} evolution compared to Site 1051B, which is indeed documented in Figure 2. The contrasting North Atlantic ε_{Nd} records (Figure 2c) also support model predictions (Winguth et al., 2010) that the North Atlantic was well-stratified until after the PETM, which is reflected by the convergence of the Nd isotope records indicating more efficient vertical mixing. This stratification was potentially interrupted briefly near the onset of the PETM. Specifically, ε_{Nd} signatures from fish teeth from site 401 indicate the Atlantic may have experienced rapid circulation changes early in the PETM (Figure 1) with ε_{Nd} briefly shifting from ~ -9 to ~-10. A caveat is that while it is possible that bathymetric barrier impeded exchange within the Atlantic, the isotopic composition of modern North Atlantic Deep Water increases by about 1 ε_{Nd} units from the North (-11.5 ε_{Nd}) to South Atlantic (-10.5 ε_{Nd}; Lacan et al., 2012), which is a similar magnitude as the offset observed in these data (< 1 ε_{Nd} unit).

3.3.3. Pacific Ocean records

The distinct ε_{Nd} records of the Pacific point to restricted Pacific intermediate water mass exchange with the "Southern Ocean" (Figure 3). In this case, a possible barrier preventing substantial exchange between the Southern Ocean and Pacific Ocean might have been the shallow seas between southern Asia and Australia (Bice and Marotzke, 2002). Within the Pacific Ocean, times of convergent ε_{Nd} can be explained by a weakened southern Pacific ventilation which would allow northern Pacific water to influence both sites. With intensified Southern Ocean sourced ventilation, Pacific Site 1220B ε_{Nd} would have diverged from the signatures of the northern source (Bice and Marotzke, 2002).

317 It follows that a Pacific circulation pattern, consistent with both $\delta^{13}C$ and ε_{Nd} data, must
318 involve distinct southern- and northern-Pacific sources of deep waters, as predicted in previous
319 studies (Lunt et al., 2011; Thomas, 2004; Thomas et al., 2008; Winguth et al., 2010). A sudden
320 shift in the ε_{Nd} record at site 1220 immediately prior to the PETM may reflect the sudden onset
321 of deep-water formation in the North Pacific (Figure 3). The initial change in ε_{Nd} from ~ -4 to ~
322 -6 at Site 1220B is recorded stratigraphically below the negative carbon isotope excursion,
323 consistent with the hypothesis that circulation changes triggered PETM carbon release.
324 Alternatively, the more negative ε_{Nd} at the beginning of the PETM may reflect a dramatic change
325 in ventilation from a southern source that occurred just prior to the PETM. Also possible, the ε_{Nd}
326 record at site 1220 may record significant changes in deep-ocean redox conditions due to its
327 abyssal location in the tropical Pacific and the well-documented changes in dissolved
328 oxygenation at the onset of the PETM. In that case, this Nd isotope shift might simply reflect the
329 progression of a redox front in sediments. Unfortunately, no additional samples are available
330 from site 1220B to further investigate these trends.
331 However several factors suggest this Nd isotope shift reflects changes in bottom water
332 sourcing and not changes in the position of a sediment redox front. First, a ventilation change in
333 the deep Pacific is in agreement with interpretations of carbon isotope data that support a
334 reversal or large change in deep-water aging gradients between basins (Tripati and Elderfield,
335 2005). Secondly, carbonate geochemical data exist which suggest a reversal or dramatic change
336 in deep ocean carbonate saturation gradients between basins, consistent with a circulation change
337 (Zeebe and Zachos, 2007). Thirdly, substantially larger redox changes are observed in PETM
338 sequences from other basins (i.e., the South Atlantic; Chun et al., 2010) that do not exhibit

339 similar corresponding shifts in records of ε_{Nd}. Fourthly, similar types of changes are observed
340 during Cretaceous ocean anoxic events (Martin et al., 2012) where there also is no clear-cut
341 evidence for redox fronts driving the sediment leachate ε_{Nd} record. Finally, core photographs
342 show that transitions in sediment redox at Site 1220B are not directly coincident with the ε_{Nd}
343 change.

344 Thus we conclude these Nd isotope data are consistent with proxy data (Nunes and
345 Norris, 2006; Tripati and Elderfield, 2005; Zeebe and Zachos, 2007) and models (Bice and
346 Marotske, 2002; Lunt et al, 2011) and reflect a circulation change at the PETM. These data may
347 record a Pacific circulation 'trigger' for carbon release. Some simulations indicate that at the
348 PETM, a change in state of a Southern Pacific deep-water source could contribute to hydrate
349 destabilization, which these data may reflect. Such changes in Southern Ocean water mass
350 characteristics could ultimately have arisen from a gradual forcing such as volcanic outgassing
351 (Kennett and Stott, 1991; Bice and Marotske, 2002; Lunt et al., 2011; Tripati and Elderfield,
352 2005).

353

354 **CONCLUSIONS**

355 Our study provides new neodymium isotope data from Fe-Mn leachates constraining
356 changes in ocean circulation associated with the PETM. The novelty of these Nd isotope data
357 reflect advances in our ability to extract such data from pelagic sediments, which has opened
358 new avenues of paleoceanographic research. Using Nd isotopes, a proxy independent of carbon
359 cycle processes, we unravel oceanographic changes during the PETM and are able to isolate
360 competing factors controlling the carbon-isotope record during the PETM. In general, we find

these data are similar to results from fish teeth (a more widely used proxy), and discuss the combined high-resolution records for seven sites.

The high-resolution combined Nd isotope records provide further evidence for changes in thermohaline circulation associated with the PETM, as previously inferred from basinal carbon isotope gradients (Nunes and Norris, 2006; Tripati and Elderfield, 2005) and constraints on deep-water carbonate ion concentrations (Zeebe and Zachos, 2007). In addition, these new records provide additional constraints on the timing and the nature of changes in circulation. The records are consistent with variations in bottom water mass mixing in each basin associated with the PETM, with water mass distributions implying intermediate and deep-water circulation changes. We find that changes in deep ocean circulation occurred during the Paleocene-Eocene, and that these circulation changes likely preceded the carbon release, based on ε_{Nd} shifts observed stratigraphically below the carbon isotope excursion. Together with modeling results (Bice and Marotzke, 2002; Lunt et al., 2011, 2012; Winguth et al., 2010) and Mg/Ca-based bottom water temperature estimates (Tripati and Elderfield, 2005), Nd isotope data provide further evidence for thermohaline changes that may have served as a "trigger" of carbon release.

ACKNOWLEDGEMENTS

Samples were provided by the Integrated Ocean Drilling Program. NSF grant 1147407 supported the contributions of A.N.A. A.T. was supported by a NERC Fellowship, a Junior Research Fellowship from Magdalene College, and the UCLA Division of Physical Sciences, and thanks Alex Piotrowski for discussing this work and making some pilot measurements. C. Teschner, R. Stumpf and J. Heinze are acknowledged for laboratory support and F. Hauff is thanked for technical support of the mass spectrometer at GEOMAR, Kiel. This work was also supported by

384 the "Laboratoire d'Excellence" LabexMER (ANR-10-LABX-19) and co-funded by a grant from
385 the French government under the program "Investissements d'Avenir".
386

387 **REFERENCES CITED**

388

389 Alexander, K., Meissner, K.J., Bralower, T.J., 2015. Sudden spreading of corrosive bottom
390 water during the Palaeocene-Eocene Thermal Maximum. Nat. Geo., **8**, 458-462. DOI:
391 10.1038/NGEO2430.
392 Bayon, G., German, C., Boella, R., Milton, J., Taylor, R., Nesbitt, R., 2002. An improved
393 method for extracting marine sediment fractions and its application to Sr and Nd isotopic
394 analysis. Geochim. Cosmochim. Acta, v. 187, p. 170–199.
395 Bayon, G., German, C.R., Burton, K.W., Nesbitt, R.W., & Rogers, N., 2004. Sedimentary Fe-
396 Mn oxyhydroxides as paleoceanographic archives and the role of Aeolian flux in regulating
397 oceanic dissolved REE. Earth and Planetary Science Letters, v. 224, p 477-492, doi:
398 10.1016/j.epsl.2004.05.033
399 Bice, K.L. & Marotzke, J., 2002, Could changing ocean circulation have destabilized methane
400 hydrate at the Paleocene/Eocene boundary? Paleoceanography, v. 17, p.1018,
401 doi.10.1029/2001pa000678.
402 Böhm, E., Lippold, J., Gutjahr, M., Frank, M., Blaser, P., Antz, B., Fohlmeister, J., Frank, N.,
403 Andersen, M.B., & Deininger, M., 2015. Strong and deep Atlantic meridional
404 overturning circulation during the last glacial cycle. Nature, v.517, doi:
405 10.1038/nature14059

406 Bowen, G. J., Beerling, D. J., Koch, P. L., Zachos, J. C., & Quattlebaum, T., 2004. A humid
407 climate state during the Palaeocene/Eocene thermal maximum. *Nature*, v. *432*(7016), p. 495-
408 499.
409 Bowen, G. J., Koch, P. L., Gingerich, P. D., Norris, R. D., Bains, S., & Corfield, R. M., 2001.
410 Refined isotope stratigraphy across the continental Paleocene-Eocene boundary on Polecat
411 Bench in the northern Bighorn Basin.*Paleocene-Eocene stratigraphy and biotic change in*
412 *the Bighorn and Clarks Fork basins, Wyoming. University of Michigan Papers on*
413 *Paleontology*, v. *33*, p. 73-88.
414 Chun, C. O., Delaney, M. L., & Zachos, J. C., 2010. Paleoredox changes across the Paleocene-
415 Eocene thermal maximum, Walvis Ridge (ODP Sites 1262, 1263, and 1266): Evidence from
416 Mn and U enrichment factors. Paleoceanography, 25(4), DOI: 10.1029/2009PA001861.
417 Cope, J.T. & Winguth, A., 2011, On the sensitivity of ocean circulation to arctic freshwater input
418 during the Paleocene/Eocene Thermal Maximum. Palaeogeography, Palaeoclimatology,
419 Palaeoecology, v. 306, p. 82-94.
420 Cramer, B.S. & Kent, D.V., 2005, Bolide summer: The Paleocene/Eocene thermal maximum as
421 a response to an extraterrestrial trigger. Palaeogeography, Palaeoclimatology,
422 Palaeoecology, v. 224, p. 144-166, doi.10.1016/J.Paleo.2005.03.040.
423 Dickens, G.R., O'Niel, J.R., Rea, D.K., & Owen, R.M., 1995, Dissociation of oceanic methane
424 hydrate as a cause of the carbon isotope excursion at the end of the Paleocene.
425 Paleoceanography, v. 10, p. 965-971.
426 Dickens, G.R., 2000. Methane oxidation during the late Paleocene thermal maximum. Bulletin
427 de la Société Géologique de France, v. 171, p. 37-49.

Farley, K.A. & Eltgroth, S.F., 2003, An alternative age model for the Paleocene-Eocene thermal maximum using extraterrestrial ^{3}He. Earth and Planetary Science Letters, v. 208, p.135-148.

Frank, M., 2002, Radiogenic isotopes: Tracers of part ocean circulation and erosional input. Review of Geophysics, v. 40(1), p.1001, doi.10.1029/2000RG000094.

Goldstein, S.L., Hemming, S.R., Heinrich, D.H., & Karl, K.T., 2003, Long-lived Isotopic Tracers in Oceanography, Paleoceanography, and Ice-sheet Dynamics. Treatise on Geochemistry (ed. Elderfield, H.) 453-489.

Gutjahr, M., *et al*., 2007, Reliable extraction of a deepwater trace metal isotope signal from Fe-Mn oxyhydroxide coatings of marine sediments. Chemical Geology, v. 242, p. 351-370, doi.10.1016/J.Chemgeo.2007.03.021.

Haley, B.A., Frank, M., Spielhagen, R.F., & Fietzke, J., 2008a, Radiogenic isotope record of Arctic Ocean circulation and weathering inputs of the past 15 million years. Paleoceanography, v. 23, doi.10.1029/2007PA001486.

Haley, B.A., Frank, M., Spielhagen, R.F., & Eisenhauer, A., 2008b, Influence of brine formation on Arctic Ocean circulation over the past 15 million years. Nature Geoscience, v. 1, p. 68-72, doi.10.1038/Ngeo.2007.5.

Higgins, J.A. & Schrag, D.P., 2006, Beyond methane: Towards a theory for the Paleocene-Eocene Thermal Maximum. Earth and Planetary Science Letters, v. 245, 523-537, doi.10.1016/JEpsl.2006.03.009.

Huber, M., & Sloan, L.C., 2001, Heat transport, deep waters, and thermal gradients: Coupled simulation of an Eocene Greenhouse Climate. Geophysical Research Letters, v. 28, p. 3481-3484.

450 Jacobsen, S.B. & Wasserburg, G.J., 1979, Mean Age of Mantle and Crustal Reservoirs. Journal
451 of Geophysical Research, v. 85, p. 7411-7427.
452 Katz, M.E., Pak, D.K., Dickens, G.R., & Miller, K.G., 1999. The source and fate of massive
453 carbon input during the latest Paleocene thermal maximum. Science, v. 286, p. 1531-1533.
454 Kennett, J.P. & Stott, L.D., 1991, Abrupt deep-sea warming, palaeoceanographic changes and
455 benthic extinctions at the end of the Palaeocene. Nature, v. 353, p. 225-229.
456 Khélifi, N., and Frank, M., 2014. A major change in North Atlantic deep water circulation 1.6
457 million years ago. Climates of the Past, v. 10, p 1441-1451. doi 10.5194/cp-10-1441-2014
458 Koch, P. L., Zachos, J. C., & Gingerich, P. D., 1992. Correlation between isotope records in
459 marine and continental carbon reservoirs near the Paleocene Eocene boundary. Nature, v.
460 358, p. 319-322.
461 Kump, L., Bralower, T., & Ridgewell, A., 2009. Ocean acidification in deep time.
462 Oceanography, v. 22, p 94-107.
463 Kurtz, A.C., Kump, L.R., Arthur, M.A., Zachos, J.C., & Paytan, A., 2003, Early Cenozoic
464 decoupling of the global carbon and sulfur cycles. Paleoceanography v. 18, p. 1090,
465 doi.10.1029/2003pa000908.
466 Lacan, F., Tachikawa, K., Jeandel, C., 2012, Neodymium isotopic composition of the oceans: A
467 compilation of seawater data. Chemical Geology v 300-301, 177-184.
468 Lunt, D.J., Ridgwell, A., Sluijs, A., Zachos, J., Hunter, S., & Haywood, A., 2011, A model for
469 orbital pacing of methane hydrate destabilization during the Palaeogene. Nature Geoscience,
470 v. 4, p. 775-778, doi.10.1038/Ngeo1266.
471 Lunt, D. J., Dunkley Jones, T., Heinemann, M., Huber, M., LeGrande, A., Winguth, A., Loptson,
472 C., Marotzke, J., Roberts, C. D., Tindall, J., Valdes, P., and Winguth, C., 2012, A model-data

comparison for a multi-model ensemble of early Eocene atmosphere-ocean simulations: EoMIP, Clim. Past, v. 8, p.1717-1736, doi:10.5194/cp-8-1717-2012.

Martin, E.E., Blair, S.W., Kamenov, G.D., Scher, H.D., Bourbon, E., Basak, C., and Newkirk, D.N., 2010. Extraction of Nd isotopes from bulk deep sea sediments for paleoceanographic studies on Cenozoic time scales. Chem. Geol., v. 269, p. 414-431.

Martin, E.E., MacLeod, K.G., Berrocoso, A.J., & Bourbon, E., 2012. Water mass circulation on Demerara Rise during the Late Cretaceous based on Nd isotopes. Earth and Planetary Science Letters, v. 327-328, p. 111-120.

McCarren, H., Thomas, E., Hasegawa, T., Rohl, U., & Zachos, J.C., 2008, Depth dependency of the Paleocene-Eocene carbon isotope excursion: Paired benthic and terrestrial biomarker records (Ocean Drilling Program Leg 208, Walvis Ridge). Geochemistry Geophysics Geosystems, v. 9, doi.10.1029/2008gc002116: Q10008.

McInerney, F.A., Wing, S.L., 2011. The Paleocene-Eocene Thermal Maximum: A Perturbation of Carbon Cycle, Climate, and Biosphere with Implications for the Future, Annual Review of Earth and Planetary Sciences, v. 39, p. 489-516.

Molina-Kescher, M., Frank, M., and Hathorne, E., 2014. South Pacific dissolved Nd isotope compositions and rare earth element distributions: Water mass mixing versus biogeochemical cycling. Geochimica et Cosmochimica Acta, v. 127, p 171-189. doi: 10.1016/j.gca.2013.11.038

Murphy, B.H., Farley, K.A., & Zachos, J.C., 2010, An extraterrestrial ^{3}He-based timescale for the Paleocene-Eocene thermal maximum (PETM) from Walvis Ridge, IODP Site 1266. Geochimica et Cosmochimica Acta, v. 74, p. 5098-5108.

Nunes, F. & Norris, R.D., 2006, Abrupt reversal in ocean overturning during the Palaeocene/Eocene warm period. Nature, v. 439, p. 60-63, doi.10.1038/Nature04386.

Pagani, M., Pedentchouk, N., Huber, M., Sluijs, A., Schouten, S., Brinkhuis, H., Sinnghe-Damste, J., & Dickens, G. R., 2006. Arctic hydrology during global warming at the Palaeocene/Eocene thermal maximum. Nature, v. 442(7103), p. 671-675.

Paytan, A., Averyt, K., Faul, K., Gray, E., and Thomas, E., 2007, Barite accumulation, ocean productivity, and Sr/Ba in barite across the Paleocene-Eocene Thermal Maximum: Geology, v. 35, p. 1139-1142, doi: 10.1130/G24162A.1.

Piotrowski, A. M., Goldstein, S. L., Hemming, S. R., & Fairbanks, R. G., 2004. Intensification and variability of ocean thermohaline circulation through the last deglaciation. Earth and Planetary Science Letters, 225(1), 205-220.

Piotrowski, A.M., Goldstein, S.L., Hemming, S.R., & Fairbanks, R.G., 2005, Temporal relationships of carbon cycling and ocean circulation at glacial boundaries. Science, v. 307, p.1933-1938, doi.10.1126/Science.1104883.

Piotrowski, A. M., Goldstein, S. L., Hemming, S., Fairbanks, R. G., & Zylberberg, D. R., 2008. Oscillating glacial northern and southern deep water formation from combined neodymium and carbon isotopes. Earth and Planetary Science Letters, 272(1), 394-405.

Ridgewell, A., & Schmidt, D.N., 2010. Past constraints on the vulnerability of marine calcifiers to massive carbon dioxide release. Nature Geosciene, v. 3., p. 196-200.

Röhl, U., Westerhold, T., Bralower, T.J., & Zachos, J.C., 2007, On the duration of the Paleocene-Eocene thermal maximum (PETM). Geochemistry Geophysics Geosystems, v. 8, Q12002.

Rutberg, R.L., Hemming, S.R., & Goldstein, S.L., 2000, Reduced North Atlantic Deep Water flux to the glacial Southern Ocean inferred from neodymium isotope ratios. Nature, v. 405, p. 935-938.

Scher, H.D., & Martin, E.E., 2006, Timing and climatic consequences of the opening of Drake Passage. Science, v. 312, p. 428-430, doi.10.1126/Science.1120044.

Sluijs, A., Schouten, S., Pagani, M., Woltering, M., Brinkhuis, H., Damsté, J. S. S., Dickens, J. & Moran, K., 2006. Subtropical Arctic Ocean temperatures during the Palaeocene/Eocene thermal maximum. Nature, v. 441(7093), p. 610-613.

Sluijs, A., Brinkhuis, H., Schouten, S., Bohaty, S.M., John, C.M., Zachos, J.C., Reichart, G.-J., Sinninghe Damsté, J. S., Crouch, E.M., and Dickens, G.R., 2007, Environmental precursors to rapid light carbon injection at the Palaeocene/Eocene boundary. Nature, v. 450, p. 1218-1221.

Stichel, T., Frank., M., Rickli, J., & Haley, B.A., 2012, The hafnium and neodymium isotope composition of seawater in the Atlantic sector of the Southern Ocean. Earth and Planetary Science Letters, v. 317-318, p. 282-294.

Storey, M., Duncan, R.A., & Swisher, C.C., 2007, Paleocene-Eocene thermal maximum and the opening of the northeast Atlantic. Science, v. 316, p. 587-589, doi.10.1126/Science.1135274.

Svensen, H., Planke, S., Malthe-Sørenssen, A., Jamtveit, B., Myklebust, R., Eidem, T. R., & Rey, S. S., 2004, Release of methane from a volcanic basin as a mechanism for initial Eocene global warming. Nature, v. 429, p. 542-545, doi.10.1038/Nature02566.

538 Thomas, D.J., Zachos, J.C., Bralower, T.J., Thomas, E., & Bohaty, S., 2002, Warming the fuel
539 for the fire: Evidence for the thermal dissociation of methane hydrate during the Paleocene-
540 Eocene thermal maximum. Geology, v. 30, p. 1067-1070.
541 Thomas, D.J., Bralower, T.J., & Jones, C.E., 2003, Neodymium isotopic reconstruction of late
542 Paleocene-early Eocene thermohaline circulation. Earth and Planetary Science Letters, v
543 209, p. 309-322, doi.10.1016/S0012-821x(03)00096-7.
544 Thomas, D.J., 2004, Evidence for deep-water production in the North Pacific Ocean during the
545 early Cenozoic warm interval. Nature, v. 430, p. 65-68, doi.10.1038/nature02639.
546 Thomas, D.J., Lyle, M., Moore, T.C., & Rea, D.K., 2008, Paleogene deepwater mass
547 composition of the tropical Pacific and implications for thermohaline circulation in a
548 greenhouse world. Geochemistry Geophysics Geosystems, v. 9, doi.Q02002
549 10.1029/2007gc001748.
550 Thomas, D.J., Korty, R., Huber M., Schubert, J.A., Haines, B., 2014. Nd isotopic structure of
551 the Pacific Ocean 70-30 Ma and numerical evidence for vigorous ocean circulation and
552 ocean heat transport in a greenhouse world. *Paleoceanography*, **29**, 454–469,
553 doi:10.1002/2013PA002535.
554 Tripati, A.K. & Elderfield, H., 2004, Abrupt hydrographic changes in the equatorial Pacific and
555 subtropical Atlantic from foraminiferal Mg/Ca indicate greenhouse origin for the thermal
556 maximum at the Paleocene-Eocene Boundary. Geochemistry Geophysics Geosystems, v. 5,
557 Q02006.
558 Tripati, A. & Elderfield, H., 2005, Deep-sea temperature and circulation changes at the
559 Paleocene-Eocene thermal maximum. Science, v. 308, p. 1894-1898,
560 doi.10.1126/Science.1109202.

Wilson, D.J., Piotrowski, A.M., Galy, A., and McCave, I.N., 2012. A boundary exchange influence on deglacial neodymium isotope records from the deep western Indian Ocean. Earth and Planetary Science Letters, v 341-344, p 35-47. doi: 10.106/j.epsl.2012.06.009

Winguth, A., Shellito ,C., Shields, C., & Winguth, C., 2010, Climate Response at the Paleocene-Eocene Thermal Maximum to Greenhouse Gas Forcing-A Model Study with CCSM3. Journal of Climatology, v. 23, p. 2562-2584, doi.10.1175/2009jcli3113.1.

Zachos, J., Pagani, M., Sloan, L., Thomas, E., & Billups, K., 2001, Trends, rhythms, and aberrations in global climate 65 Ma to present. Science, v. 292, p. 686-693.

Zachos JC*, et al*., 2003, A transient rise in tropical sea surface temperature during the Paleocene-Eocene Thermal Maximum. Science, v. 302, p. 1551-1554, doi.10.1126/Science.1090110.

Zachos, J.C., Röhl, U., Schellenberg, S.A., Sluijs, A., Hodell, D.A., Kelly, D.C., Thomas, E., Nicolo, M., Raffi, I., Lourens, L.J., McCarren, H., & Kroon, D., 2005. Rapid Acidification of the Ocean During the Paleocene-Eocene Thermal Maximum. Science, v. 308, p. 1611-1615.

Zachos, J. C., Schouten, S., Bohaty, S., Quattlebaum, T., Sluijs, A., Brinkhuis, H., Gibbs, S. & Bralower, T. J., 2006. Extreme warming of mid-latitude coastal ocean during the Paleocene-Eocene Thermal Maximum: Inferences from TEX86 and isotope data. *Geology* v. 34, no. 9, p. 737-740.

Zachos, J.C., Dickens, G.R., & Zeebe, R.E., 2008. An early Cenozoic perspective on greenhouse warming and carbon-cycle dynamics. Nature, v. 451, p. 279-283.

Zeebe, R.E. & Zachos, J.C., 2007, Reversed deep-sea carbonate ion basin gradient during Paleocene-Eocene thermal maximum. Paleoceanography, v. 22, p. 3201.

583 Zeebe, R.E., Zachos, J.C., & Dickens, G.R., 2009, Carbon dioxide forcing alone insufficient to
584 explain Palaeocene-Eocene Thermal Maximum warming. Nature Geoscience, v. 2, p. 576-
585 580, doi.10.1038/ngeo578.
586
587
588
589
590
591

Figure Captions:

Figure 1: Sediment leach ε_{Nd} and available fish teeth ε_{Nd} data from 55.1 to 55.4 Ma for all three ocean basins. Sediment ε_{Nd} values are connected with a dotted line and fish teeth data are represented by unconnected dots. The green shaded area represents the PETM as marked by the carbon isotope excursion from each core. These data sources are generally consistent, although higher-order differences, likely intrinsic to the natures of the archival sources, are present.

Figure 2: Nd and C isotope data (ε_{Nd} and $\delta^{13}C$) across the PETM from the Southern Ocean (a), Pacific Ocean (b), and Atlantic Basins (c). The sediment leach ε_{Nd} are shown with circles and solid lines; the fish teeth/debris ε_{Nd} from Thomas et al. (2003) are shown as dots. All data are presented on directly comparable scales for both ε_{Nd} and $\delta^{13}C$. The sample ages are based on the $\delta^{13}C$ age models. In (b) the age model of Site 1209B has been slightly adjusted (second x axis) such that the $\delta^{13}C$ excursion coincides with the age of the PETM in the other cores. The shaded vertical bar indicates the timing of the PETM as defined by the CIE in the cores.

Figure 3: A conceptual model of the intermediate/deep-water mixing changes across the PETM as inferred from ε_{Nd} records of intermediate/deep-water mass geometries. Arrow boldness reflects overturning circulation that could produce water mass geometries. Dashed arrows represent weak overturning. *Italicized numbers* indicate the interpreted ε_{Nd} from each site for the time period. The arrow directions reflect our interpretation of the general direction of flow, and are not meant to be viewed as precise flow-paths. The paleogeographic distribution of the continents is from Ocean Drilling Stratigraphic Network (ODSN).

List of tables

Figure 1

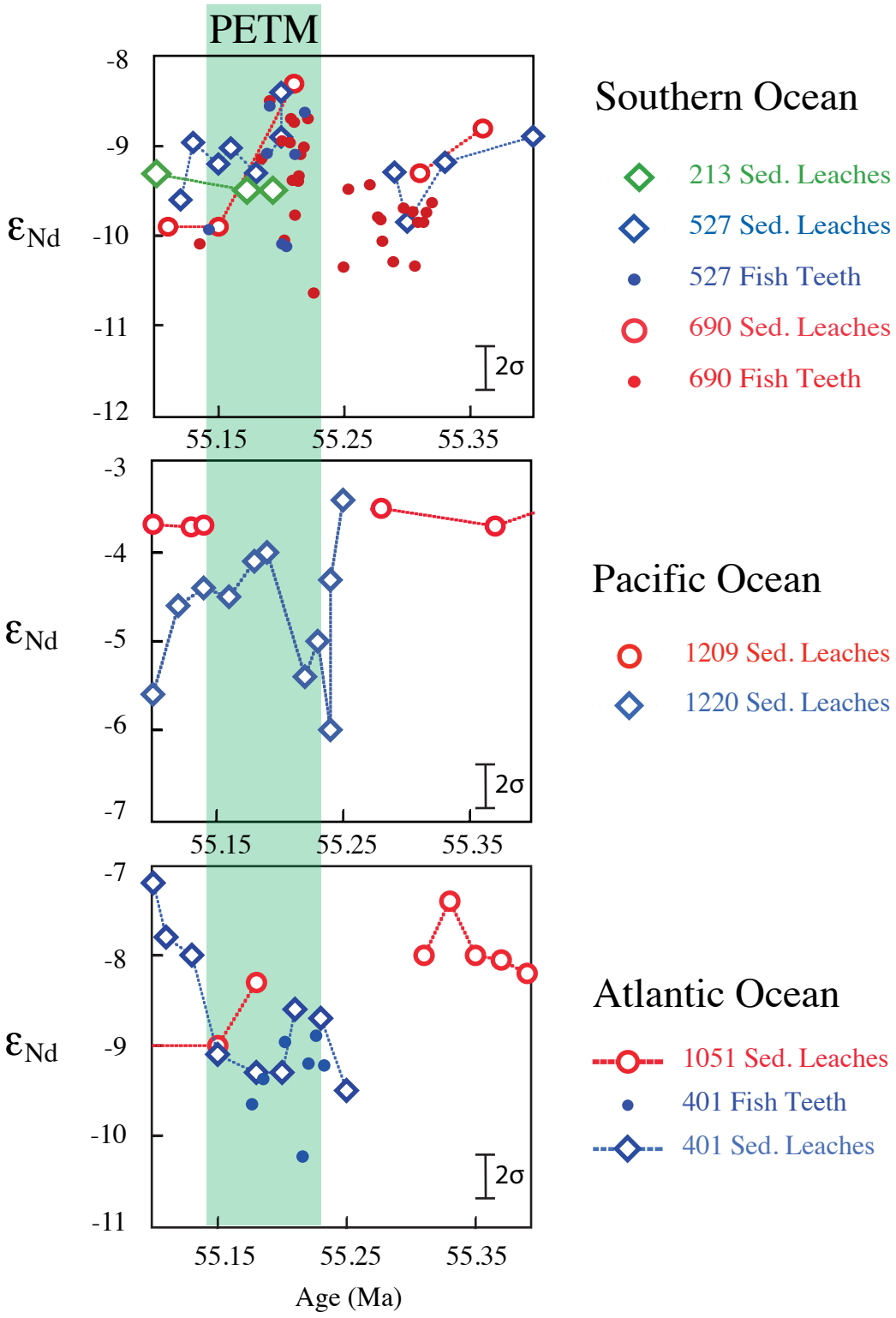
PETM
εNd
-8
-9
-10
-11
-12
55.15
55.25
55.35
2σ
-3
-4
-5
-6
-7
-7
-8
-9
-10
-11
Age (Ma)
Southern Ocean
213 Sed. Leaches
527 Sed. Leaches
527 Fish Teeth
690 Sed. Leaches
690 Fish Teeth
Pacific Ocean
1209 Sed. Leaches
1220 Sed. Leaches
Atlantic Ocean
1051 Sed. Leaches
401 Fish Teeth
401 Sed. Leaches

Figure 2

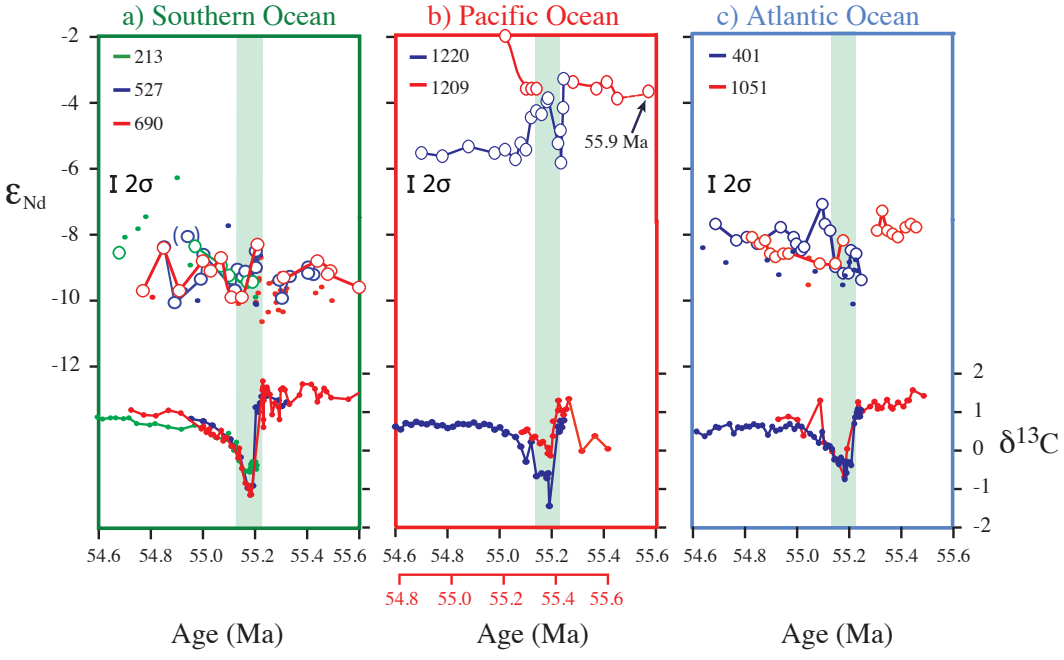
a) Southern Ocean
b) Pacific Ocean
c) Atlantic Ocean
213
527
690
1220
1209
401
1051
55.9 Ma
I 2σ
εNd
δ13C
-2
-4
-6
-8
-10
-12
2
1
0
-1
-2
54.6
54.8
55.0
55.2
55.4
55.6
Age (Ma)

Figure 3

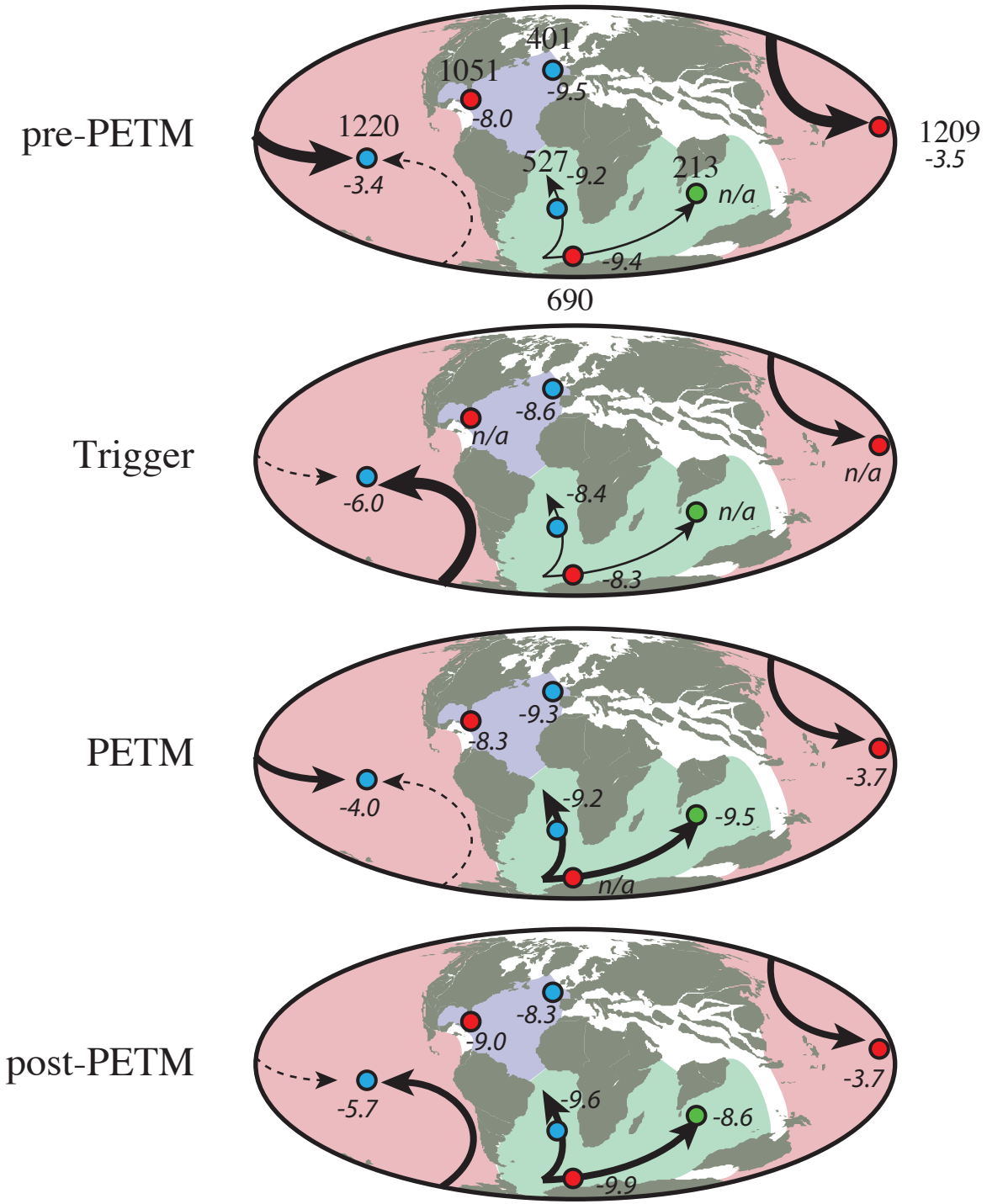
pre-PETM
401
1051
-9.5
-8.0
1220
-3.4
527
-9.2
213
n/a
-9.4
1209
-3.5
690
Trigger
-8.6
n/a
-6.0
-8.4
n/a
n/a
-8.3
PETM
-9.3
-8.3
-4.0
-9.2
-9.5
-3.7
n/a
post-PETM
-8.3
-9.0
-5.7
-9.6
-8.6
-3.7
-9.9

Table 1 Site Descriptions

Core	Modern Latitude and Longitude and depth (m)			Paleo-Depth (m)	$\delta^{13}C$ data reference
213	10°12.7'S	93°53.8'E	5601	3000	Thomas et al., 2003
401	47°25.7'N	8°48.6'W	2495	1900	Thomas et al., 2003
527	28° 2.5'S	1°45.8'E	4428	3400	Thomas et al., 2003
690B	65° 9.6'S	1°12.3'E	2914	1900	Thomas et al., 2003
1051B	30° 3.2'N	76°21.5'W	1981	2000	Thomas et al., 2003
1209B	32°39.1'N	158°30.4'E	2387	2400	Tripati and Elderfield, 2005
1220B	10°10.6'N	142°45.5'W	5218	3200	Tripati and Elderfield, 2005

Table 2 Sample Description and ε_{Nd}

Hole	Core Section	Depth Interval (cm)		ε_{Nd}	age Ma
		upper	lower		
1220B	20X-1	65	67	**-5.70**	54.70
1220B	20X-1	85	87	**-5.80**	54.78
1220B	20X-1	110	112	**-5.50**	54.88
1220B	20X-1	135	137	**-5.70**	54.98
1220B	20X-1	145	147	**-5.60**	55.02
1220B	20x-2	5	7	**-5.90**	55.06
1220B	20x-2	10	12	**-5.40**	55.08
1220B	20x-2	15	17	**-5.60**	55.10
1220B	20x-2	20	22	**-4.60**	55.12
1220B	20x-2	25	27	**-4.40**	55.14
1220B	20x-2	30	32	**-4.50**	55.16
1220B	20x-2	35	37	**-4.10**	55.18
1220B	20x-2	40	42	**-4.00**	55.19
1220B	20x-2	80	82	**-5.40**	55.22
1220B	20x-2	90	92	**-5.00**	55.23
1220B	20x-2	93	94	**-6.00**	55.24
1220B	20x-CCW	5	6	**-4.31**	55.24
1220B	20x-CCW	6	7	**-3.41**	55.25
1209B	22H-1	12	14	**-2.10**	55.02
1209B	22H-1	39	40	**-3.68**	55.10
1209B	22H-1	47	48	**-3.71**	55.13
1209B	22H-1	48	49	**-3.69**	55.14
1209B	22R-1	84	86	**-3.50**	55.28
1209B	22R-1	108	110	**-3.70**	55.37
1209B	22R-1	120	122	**-3.50**	55.41
1209B	22R-1	132	134	**-4.00**	55.45
1209B	22R-1	148	150	**-3.70**	55.85
0690B	18H-5	36	37	**-9.70**	54.77
0690B	18H-6	30	31	**-8.40**	54.84
0690B	18H-6	110	111	**-9.70**	54.91
0690B	19H-1	30	31	**-8.80**	55.00
0690B	19H-1	65	66	**-9.10**	55.03
0690B	19H-1	137	138	**-8.70**	55.07
0690B	19H-2	47	48	**-9.90**	55.11
0690B	19H-2	109	110	**-9.90**	55.15
0690B	19H-3	69	71	**-8.30**	55.21
0690B	19H-4	66	67	**-9.30**	55.31
0690B	19H-5	6	7	**-8.80**	55.36
0690B	19H-5	65	66	**-9.10**	55.44
0690B	19H-5	106	107	**-9.20**	55.48
0690B	20H-1	3	4	**-9.63**	55.53
0690B	20H-1	140	141	**-9.84**	55.80
0690B	20H-2	111	112	**-9.20**	56.17
527	24R-1	11	12	**-8.27**	54.85
527	24R-1	31	32	**-9.98**	54.89
527	24R-1	53	54	**-7.95**	54.94
527	24R-1	81	82	**-9.26**	54.99
527	24R-1	100	102	**-8.50**	55.00
527	24R-1	140	142	**-9.60**	55.12
527	24R-2	11	12	**-8.96**	55.13
527	24R-2	41	42	**-9.20**	55.15
527	24R-2	87	88	**-9.02**	55.16
527	24R-2	24	27	**-9.30**	55.18
527	24R-2	30	33	**-8.90**	55.20
527	24R-2	47	48	**-8.40**	55.20
527	24R-3	59	60	**-9.29**	55.29
527	24R-3	81	82	**-9.85**	55.30
527	24R-3	121	122	**-9.18**	55.33
527	24R-4	10	11	**-8.89**	55.40
527	24R-4	40	41	**-9.12**	55.42
527	24R-4	80	81	**-9.08**	55.40
213	16-3	48	49	**-8.60**	54.69
213	16-4	8	9	**-8.40**	54.97
213	16-4	49	50	**-9.00**	55.08
213	16-4	58	59	**-9.30**	55.10
213	16-4	90	91	**-9.50**	55.17
213	16-4	99	100	**-9.50**	55.19
1051B	59X-2	110	111	**-8.23**	54.50
1051B	59X-2	139	140	**-8.41**	54.60
1051B	59X-3	26	27	**-8.26**	54.76
1051B	59X-3	46	47	**-8.65**	54.80
1051B	59X-3	67	68	**-8.81**	54.90
1051B	59X-3	87	88	**-8.75**	54.94
1051B	59X-3	120	120	**-8.70**	54.97
1051B	60X-1	65	65	**-9.00**	55.09
1051B	60X-1	119	120	**-9.00**	55.15
1051B	60X-1	145	145	**-8.30**	55.18
1051B	60X-2	56	56	**-8.00**	55.31
1051B	60X-2	64	66	**-7.40**	55.33
1051B	60X-2	74	75	**-8.00**	55.35
1051B	60X-2	84	85	**-8.05**	55.37
1051B	60X-2	93	94	**-8.20**	55.39
1051B	60X-2	109	110	**-7.89**	55.42
1051B	60X-2	118	119	**-7.79**	55.44
1051B	60X-2	142	143	**-7.93**	55.52
401	14R-1	45	47	**-7.80**	54.69
401	14R-1	100	101	**-8.26**	54.77
401	14R-1	125	126	**-8.24**	54.81
401	14R-1	146	147	**-8.40**	54.85
401	14R-2	50	52	**-7.90**	54.94
401	14R-2	83	85	**-8.20**	54.99
401	14R-2	91	93	**-8.40**	55.00
401	14R-2	100	102	**-8.60**	55.02
401	14R-2	110	112	**-8.50**	55.03
401	14R-2	148	150	**-7.20**	55.10
401	14R-3	6	8	**-7.80**	55.11
401	14R-3	21	23	**-8.00**	55.13
401	14R-3	31	33	**-9.10**	55.15
401	14R-3	52	54	**-9.30**	55.18
401	14R-3	84	86	**-9.30**	55.20
401	14R-3	90	92	**-8.60**	55.21
401	14R-3	122	124	**-8.70**	55.23
401	14R-3	148	150	**-9.50**	55.25

Table 3 Age model description

Core	Age model segment	Core depth (MBSF)		Curve definition	
		start	end	m	b
1209B	a	210.72	211.24	0.3539	-19.317
	b	211.26	211.40	2.5000	-472.660
213	a	145.13	147.35	0.2541	+17.727
	b	147.41	147.64	0.1193	+37.590
401	a	198.54	201.97	0.1640	+22.054
	b	202.02	202.98	0.0656	+41.922
1220B	a	197.55	199.20	0.4009	-24.697
	b	199.25	199.93	0.0955	+36.159
527	a	199.63	200.71	0.2027	+14.491
	b	200.89	202.76	0.0700	+41.129
690B	a	162.80	170.69	0.0646	+44.199
	b	170.71	170.76	0.0453	+47.528
	c	170.84	172.49	0.1923	+22.416
	d	172.95	179.80	0.1167	+35.192
1051B	a	510.17	512.35	0.1164	-4.439
	b	512.40	513.80	0.2100	-52.412